



This is a repository copy of *Compositional Dependence of Solubility/Retention of Molybdenum Oxides in Aluminoborosilicate-Based Model Nuclear Waste Glasses*.

White Rose Research Online URL for this paper:  
<http://eprints.whiterose.ac.uk/129393/>

Version: Accepted Version

---

**Article:**

Brehault, A., Patil, D., Kamat, H. et al. (6 more authors) (2018) Compositional Dependence of Solubility/Retention of Molybdenum Oxides in Aluminoborosilicate-Based Model Nuclear Waste Glasses. *Journal of Physical Chemistry B* , 122 (5). pp. 1714-1729. ISSN 1520-6106

<https://doi.org/10.1021/acs.jpccb.7b09158>

---

**Reuse**

Items deposited in White Rose Research Online are protected by copyright, with all rights reserved unless indicated otherwise. They may be downloaded and/or printed for private study, or other acts as permitted by national copyright laws. The publisher or other rights holders may allow further reproduction and re-use of the full text version. This is indicated by the licence information on the White Rose Research Online record for the item.

**Takedown**

If you consider content in White Rose Research Online to be in breach of UK law, please notify us by emailing [eprints@whiterose.ac.uk](mailto:eprints@whiterose.ac.uk) including the URL of the record and the reason for the withdrawal request.



[eprints@whiterose.ac.uk](mailto:eprints@whiterose.ac.uk)  
<https://eprints.whiterose.ac.uk/>

Compositional dependence of solubility/retention of molybdenum  
oxides in aluminoborosilicate based model nuclear waste glasses

Antoine Brehault,<sup>1</sup> Deepak Patil,<sup>2</sup> Hrishikesh Kamat,<sup>1</sup> Randall E. Youngman,<sup>3</sup>  
Lynn Thirion,<sup>3</sup> John C. Mauro,<sup>3,4</sup> Claire L. Corkhill,<sup>5</sup> John S. McCloy,<sup>2,5</sup> Ashutosh  
Goel<sup>1,\*</sup>

<sup>1</sup> Department of Materials Science and Engineering, Rutgers – The State University of New Jersey,  
Piscataway, New Jersey

<sup>2</sup> School of Mechanical & Materials Engineering and Materials Science & Engineering Program,  
Washington State University, Pullman, WA, USA

<sup>3</sup> Corning Research & Development Corporation, Corning, NY 14831, USA

<sup>4</sup> Department of Materials Science and Engineering, The Pennsylvania State University, University  
Park, PA 16802, USA

<sup>5</sup> NucleUS Immobilisation Science Laboratory, Department of Materials Science and Engineering,  
University of Sheffield, Sheffield, UK

---

\* Corresponding author:  
Email: [ag1179@soe.rutgers.edu](mailto:ag1179@soe.rutgers.edu); Ph: +1-848-445-4512

## Abstract

Molybdenum oxides are an integral component of the high-level waste streams being generated from the nuclear reactors in several countries. Although borosilicate glass has been chosen as the baseline waste form by most of the countries to immobilize these waste streams, molybdate oxyanions ( $\text{MoO}_4^{2-}$ ) exhibit very low solubility ( $\sim 1$  mol.%) in these glass matrices. In the past 3-4 decades, several studies describing the compositional and structural dependence of molybdate anions in borosilicate and aluminoborosilicate glasses have been reported in the literature, providing a basis for our understanding of fundamental science that governs the solubility and retention of these species in the nuclear waste glasses. However, there are still several open questions that need to be answered to gain an in-depth understanding of the mechanisms that control the solubility and retention of these oxyanions in glassy waste forms. This article is focused on finding answers to two such questions: (1) What are the solubility and retention limits of  $\text{MoO}_3$  in aluminoborosilicate glasses as a function of chemical composition? (2) Why is there a considerable increase in the solubility of  $\text{MoO}_3$  with incorporation of rare-earth oxides (for example,  $\text{Nd}_2\text{O}_3$ ) in aluminoborosilicate glasses? Accordingly, three different series of aluminoborosilicate glasses (compositional complexity being added in a tiered approach) with varying  $\text{MoO}_3$  concentration have been synthesized and characterized for their ability to accommodate molybdate ions in their structure (solubility) and as a glass-ceramic (retention). **The contradictory viewpoints (between different research groups) pertaining to the impact of rare-earth cations on the structure of aluminoborosilicate glasses have been discussed and their implications on the solubility of  $\text{MoO}_3$  in these glasses have been evaluated.** A novel hypothesis explaining the mechanism governing the solubility of  $\text{MoO}_3$  in rare-earth containing aluminoborosilicate glasses has been proposed.

## 1. Introduction

Owing to its ability to accommodate a plethora of ionic species in its molecular structure, glass is widely considered to be the benchmark material for long-term immobilization of complex mixed radioactive wastes. The cost of vitrifying radioactive waste is directly proportional to the volume of glass to be produced. It is therefore desirable to maximize the waste loading in glass to decrease the overall volume, without posing unacceptable risk for melter operation or long-term performance of the waste form in terms of radiation and chemical stability. One major challenge in designing advanced glass formulations with enhanced waste loadings is the low solubility of some complex ionic species, for example,  $\text{MoO}_4^{2-}$ ,  $\text{SO}_4^{2-}$ ,  $\text{CrO}_4^-$ , and  $\text{TcO}_4^-$ , in borosilicate based nuclear waste glasses. This problem impacts the design and performance of nuclear waste glasses worldwide, while the relative importance of its impact is country-specific and depends on the chemistry of each nuclear waste.<sup>1-8</sup>

Molybdenum oxides are an integral component of the high level waste streams being generated from the nuclear reactors in several countries including USA (**TRUEX<sup>plus</sup> process**),<sup>9, 10</sup> France (**reprocessing of UMo fuel from gas graphite reactors**),<sup>11-13</sup> UK,<sup>14, 15</sup> and Japan.<sup>16, 17</sup> However, distinction needs to be made as molybdenum is not one of the more important components of legacy defense waste, as the burn-ups used for production of plutonium do not produce as much Mo fission product as those burn-ups used for nuclear power.<sup>18</sup> Although borosilicate glass has been chosen as the baseline waste form by all the above-mentioned countries to immobilize their high level wastes, molybdenum oxides present in their waste streams exhibit very low solubility (~ 1 mol.%) in these glass matrices.<sup>19</sup> Further increase of  $\text{MoO}_3$  concentration in these glasses usually on cooling results in liquid-liquid phase separation and subsequent crystallization of alkali molybdate phases (for example,  $\text{Na}_2\text{MoO}_4$ ) which are highly soluble in

aqueous environments.<sup>11</sup> Therefore, considerable effort is being made to design novel glass/glass-ceramic compositions which can retain higher concentration of molybdate ions in their structure without affecting the long-term performance of the final waste form. In this regard, most of the research in UK and France is focused on designing glass compositions dissolving the maximum concentration of MoO<sub>3</sub> in their structure without crystallization of alkali molybdates (or preferring the crystallization of chemically durable, CaMoO<sub>4</sub>, based phases).<sup>4, 5, 11, 14, 15, 20, 21</sup> On the other hand, research in the USA is directed towards designing a glass-ceramic that can retain the highest possible concentration of molybdenum in glass and crystal matrices, while preventing crystallization of any poorly durable phases such as alkali molybdates.<sup>9, 10, 22</sup> While the solubility of MoO<sub>3</sub> in most of the borosilicate glass compositions is limited to ~1.5 – 1.6 mol.%, the glass-ceramic being developed in USA is expected to retain ≥ 4 mol.% MoO<sub>3</sub> in the final waste form with a crystalline phase assemblage including powellite AeMoO<sub>4</sub>, oxyapatite, (A,Ae)<sub>x</sub>Ln<sub>(10-x)</sub>Si<sub>6</sub>O<sub>26</sub>, and lanthanide borosilicate (e.g., Ln<sub>5</sub>BSi<sub>2</sub>O<sub>13</sub>), where A denotes alkali, Ae alkaline-earth, and Ln lanthanide (rare earth) metals.

In the pursuit of developing an advanced waste form with enhanced waste loading, considerable effort has been made in the past 3-4 decades to understand the fundamental science and mechanisms controlling the solubility of MoO<sub>3</sub> in borosilicate/aluminoborosilicate glasses, resulting in significant advancements in our understanding about the structure and chemistry of these glasses. However, there are still some open questions which need to be answered to gain an in-depth understanding about the compositional dependence of MoO<sub>3</sub> solubility in the aluminoborosilicate glassy waste forms. This article is focused on finding answers to two such questions described below.

- i. How do the solubility and retention limits of MoO<sub>3</sub> in aluminoborosilicate glasses vary with glass chemistry? What happens if these limits are exceeded?
- ii. Why does MoO<sub>3</sub> exhibit considerably higher solubility in rare-earth (Nd<sub>2</sub>O<sub>3</sub>) containing aluminoborosilicate glasses?

While the first question has been addressed in the literature, current understanding is qualitative in nature.<sup>4, 21, 23</sup> In this paper, we aim to present quantitative data pertaining to the solubility and retention of MoO<sub>3</sub> in aluminoborosilicate glasses as a function of glass chemistry. Regarding the second question about increase in MoO<sub>3</sub> solubility, the recent literature on this topic points to the network modifying role of Nd<sub>2</sub>O<sub>3</sub> in aluminoborosilicate glasses.<sup>20, 21</sup> However, its impact on the solubility of MoO<sub>3</sub> is still unclear.<sup>21</sup> In this paper, a new hypothesis is presented describing the impact of Nd<sub>2</sub>O<sub>3</sub> on the solubility of MoO<sub>3</sub> in aluminoborosilicate glasses.

The problem of solubility/retention of molybdenum in aluminoborosilicate glasses is also an important topic beyond its use in nuclear waste immobilization. Molybdenum electrodes are often used in commercial glass manufacturing as a lower cost alternative to SnO<sub>2</sub>.<sup>24</sup> During the glass melting process, some concentration of molybdenum from the electrodes is dissolved into the molten glass. In order to avoid the formation of Mo-containing crystalline defects, it is important not to exceed the solubility limit of molybdenum during glass melting. Hence, the dependence of Mo solubility on glass chemistry is of critical importance for ensuring high quality, defect-free industrial glass production.

In preface to the technical details, it is helpful to differentiate between two terms – “solubility” and “retention”. The true “solubility” is defined as the concentration of MoO<sub>3</sub> in glass at an established equilibrium between dissolved and atmospheric MoO<sub>3</sub>. However, the glass-making process does not necessarily allow the glass melt to reach a homogeneous equilibrium.

While a component may be dissolved in the non-crystalline liquid phase up to its solubility limit, any additional concentration could exist in the form of undissolved crystalline inclusions. We therefore define “retention” as the total concentration of molybdenum oxide that is present in both the glassy matrix and any crystalline inclusions, i.e.,  $Mo_{\text{solubility}} + Mo_{\text{crystal}}$ . Note that some authors further distinguish between water soluble and water insoluble crystalline inclusions, given the importance of aqueous chemical durability and potential cracks in waste forms.<sup>25, 26</sup> Although for the sake of simplicity, we discuss the solubility and retention of molybdenum oxides in glasses, Mo is known to exist as a tetrahedral molybdate ion  $[Mo(VI)O_4^{2-}]$  in silicate and borosilicate glass chemistries.<sup>12</sup> Therefore, any discussion pertaining to solubility or retention of molybdenum in this paper refers to molybdate ions. Furthermore, while  $Mo^{6+}$  is the prevailing oxidation state in most of the borosilicate based nuclear waste glass chemistries (due to the highly oxidizing conditions of the waste feed), other oxidation states, such as  $Mo^{3+}$ ,  $Mo^{4+}$ , and  $Mo^{5+}$ , may be present under more reducing conditions or appear transiently as a result of the concentration fluctuations under the processing conditions.<sup>27</sup> These species would inevitably create other structural elements, which may have different types of bonding to the glass network. However, most of the molybdenum in the studied glasses is expected to exist in hexavalent oxidation state, especially considering the colorless nature of the as-formed glasses. Therefore, the influence of redox states on the solubility or retention of molybdenum in borosilicate glasses will not be considered in this current study.

## **2. Experimental**

### **2.1. Design of glass compositions**

A simplified nuclear waste glass-ceramic composition comprising 11.87 Na<sub>2</sub>O – 14.15 CaO – 5.35 Al<sub>2</sub>O<sub>3</sub> – 9.74 B<sub>2</sub>O<sub>3</sub> – 5.38 Nd<sub>2</sub>O<sub>3</sub> – 46.09 SiO<sub>2</sub> – 3.29 ZrO<sub>2</sub> – 4.13 MoO<sub>3</sub> (mol. %) was chosen as the baseline for this work. The baseline composition above has been derived from the more complex GC-Mo-Li 6.25 glass-ceramic composition being considered for immobilization of a waste stream derived from aqueous reprocessing of spent nuclear fuel,<sup>9</sup> wherein simplification has been made to the composition. In the simplified baseline glass for this study, Na<sub>2</sub>O represents the total fraction of alkali oxides (Na<sub>2</sub>O+Li<sub>2</sub>O+Cs<sub>2</sub>O), CaO represents the alkaline-earth oxides (CaO+BaO+SrO), and Nd<sub>2</sub>O<sub>3</sub> represents the rare-earth oxides (Y<sub>2</sub>O<sub>3</sub>+La<sub>2</sub>O<sub>3</sub>+Ce<sub>2</sub>O<sub>3</sub>+Pr<sub>2</sub>O<sub>3</sub>+Nd<sub>2</sub>O<sub>3</sub>+Sm<sub>2</sub>O<sub>3</sub>+Eu<sub>2</sub>O<sub>3</sub>+Gd<sub>2</sub>O<sub>3</sub>).

For this work, the baseline composition was further simplified into three different series of glass compositions. The first series labeled as Na-Mo-x comprises glasses in the system 25 Na<sub>2</sub>O – 5 Al<sub>2</sub>O<sub>3</sub> – 10 B<sub>2</sub>O<sub>3</sub> – (60-x) SiO<sub>2</sub> – x MoO<sub>3</sub> (x = 0 – 4 mol. %). The glasses in this series were intentionally kept devoid of CaO to avoid competition between two network modifying cations (Na<sup>+</sup> and Ca<sup>2+</sup>) for charge balancing any AlO<sub>4</sub> and BO<sub>4</sub> units, as this would add complexity to the glass structure. In the second series labeled as Ca-Mo-y, CaO was introduced in the glass system at the expense of Na<sub>2</sub>O on an equimolar basis, resulting in a series of glasses with compositions 12.5 Na<sub>2</sub>O – 12.5 CaO – 5 Al<sub>2</sub>O<sub>3</sub> – 10 B<sub>2</sub>O<sub>3</sub> – (60-y) SiO<sub>2</sub> – y MoO<sub>3</sub> (y = 0 – 4 mol. %). The aim was to understand the influence of calcium on the solubility and retention of molybdate ions. The third series labeled as RE-Mo-z was designed with an aim of investigating the influence of rare-earth oxides on the solubility of molybdenum in these glasses, given the simultaneous presence of both Ca and Na. Therefore, 5 mol. % Nd<sub>2</sub>O<sub>3</sub> was introduced in the glass system at the expense of SiO<sub>2</sub>, resulting in compositions 12.5 Na<sub>2</sub>O – 12.5 CaO – 5 Al<sub>2</sub>O<sub>3</sub> – 5 Nd<sub>2</sub>O<sub>3</sub> – 10 B<sub>2</sub>O<sub>3</sub> – (55-z)



$\text{SiO}_2 - z \text{MoO}_3$  ( $z = 0 - 4$  mol. %). **Table S1 presents the batched compositions investigated in the present study.**

## 2.2. Synthesis by melt-quench technique

High-purity powders of  $\text{SiO}_2$  (Alfa Aesar; >99.5%),  $\text{Na}_2\text{SiO}_3$  (Alfa Aesar; >99%),  $\text{Al}_2\text{O}_3$  (Sigma Aldrich;  $\geq 98\%$ ),  $\text{H}_3\text{BO}_3$  (Alfa Aesar;  $\geq 98\%$ ),  $\text{CaCO}_3$  (Alfa Aesar;  $\geq 98\%$ ),  $\text{Nd}_2\text{O}_3$  (Alfa Aesar, 99%), and  $\text{MoO}_3$  (Alfa Aesar, 99.5%) were used as glass precursors.  **$\text{Na}_2\text{SiO}_3$  was preferred over  $\text{Na}_2\text{CO}_3$  as the precursor for  $\text{Na}_2\text{O}$  to avoid any detrimental effect of alkali carbonate on the platinum crucible.** Homogeneous mixtures of batches (corresponding to ~70 g glass) were melted in Pt-Rh crucibles in the temperature range of 1400 – 1500 °C for 1 - 2 h in air, followed by quenching of melts on a steel plate. The batch temperature was lowered with increasing  $\text{MoO}_3$  content based on the decrease in apparent viscosity of glass melts.

## 2.3. Characterization of melt-quenched samples

### 2.3.1. Crystallinity in melt-quenched samples – qualitative and quantitative analysis

The melt-quenched samples were crushed to fine powders with particle size <45  $\mu\text{m}$ . Some melt-quenched samples had a layer of salt on their surfaces. All samples were analyzed qualitatively by X-ray diffraction (XRD; PANalytical – X’Pert Pro; Cu  $K_\alpha$  target at 40 kV and 40 mA). The acquisitions were performed in the  $2\theta$  range of 10 – 90° with step size of 0.013° and dwell of 0.10 s at each step. The quantitative crystalline phase analysis of samples was performed by PANalytical X’Pert Pro XRD with a Cu- $K_\alpha$  source at 45 kV and 40 mA in the  $2\theta$  range of 10 – 90° with 0.002°  $2\theta$  step size and dwell time of 5.7 s, with 5 or 10 wt.% **ZnO (NIST SRM-674b)** included as an internal standard. The quantitative phase analysis was performed by Rietveld – Reference Intensity Ratio (RIR) method using PANalytical Highscore software.

Microstructural observations were conducted on fractured crystalline samples using a field emission – scanning electron microscope (FE-SEM; ZEISS Sigma). Energy dispersive spectroscopy (EDS; X-Max Oxford Instruments; Aztec software) was employed to perform the elemental distribution mapping in the crystalline microstructure.

The liquidus temperature of rare-earth containing glasses (RE-Mo-z) was measured using gradient furnace method following the ASTM C829-81. Briefly, glass patties were crushed into powder with particle size  $\leq 841\mu\text{m}$ . The resultant glass powder was laid in a Pt/Rh boat placed on a refractory brick and then loaded into an electric gradient furnace for measurement. **The compositional and phase analysis of the crystalline phase formed at the liquidus temperature was performed by EDS and XRD, respectively.**

### 2.3.2. Chemical analysis of melt-quenched samples

The concentration of  $\text{Na}_2\text{O}$  in the melt-quenched samples was measured by flame emission spectroscopy (PerkinElmer Flame Emission Analyst 200), while the concentration of all the remaining oxides was determined by inductively coupled plasma-optical emission spectroscopy (ICP – OES; PerkinElmer ICP-OES Optima 2000DV; PerkinElmer ICP-OES Optima 7300V). The samples with white salt phase deposited on their surfaces were washed and ultra-sonicated in acetone before the chemical analysis. **Table S2 presents the experimentally analyzed compositions.**

### 2.3.3. Structural analysis of glasses

The structure of rare-earth free glasses was studied using multi-nuclear magic angle spinning-nuclear magnetic resonance (MAS NMR) spectroscopy. MAS NMR analysis could not be performed on  $\text{Nd}_2\text{O}_3$ -containing glasses due to the strong paramagnetic effect of  $\text{Nd}^{3+}$ , leading to substantially broadened NMR spectra and the inability to resolve different resonances.

The MAS NMR spectra of  $^{11}\text{B}$  and  $^{23}\text{Na}$  were acquired using commercial spectrometers (VNMRs, Agilent) and MAS NMR probes (Agilent). The samples were powdered in an agate mortar, packed into 3.2 mm zirconia rotors, and spun at 20 kHz for  $^{11}\text{B}$  MAS NMR and 22 kHz for  $^{23}\text{Na}$  MAS NMR.  $^{23}\text{Na}$  MAS NMR data was collected at 16.4 T (185.10 MHz resonance frequency), using a  $0.6\ \mu\text{s}$  ( $\sim\pi/12$  tip angle) pulse width for uniform excitation of the resonances. A range of 400 to 1000 acquisitions were co-added and the recycle delay between scans was 2 s.  $^{11}\text{B}$  MAS NMR experiments were conducted at 11.7 T (160.34 MHz resonance frequency), incorporating a 4 s recycle delay, short radio frequency (RF) pulses ( $0.6\ \mu\text{s}$ ) corresponding to a  $\pi/12$  tip angle, and signal averaging of 400 to 1000 scans. The acquired spectra were processed with minimal apodization and referenced to aqueous boric acid (19.6 ppm) and aqueous NaCl (0 ppm), respectively. Fitting of the MAS NMR spectra was performed using DMFit,<sup>28</sup> and the CzSimple model, accounting for distributions in the quadrupolar coupling constant, was utilized for  $^{23}\text{Na}$  MAS NMR spectra. The “Q MAS  $\frac{1}{2}$ ” and Gaus/Lor functions were used to fit 3- and 4-fold coordinated boron resonances in the  $^{11}\text{B}$  MAS NMR data, respectively, and  $N_4$  was calculated from the relative areas of these peaks, with a small correction due to the overlapping satellite transition of the 4-fold coordinated boron peak.<sup>29</sup>

$^{27}\text{Al}$  MAS NMR experiments on glasses were conducted at 16.4 T using a commercial spectrometer (VNMRs, Agilent) and a 1.6-mm MAS NMR probe (Agilent) with spinning speeds of 25 kHz. MAS NMR data were acquired using RF pulses of  $0.6\ \mu\text{s}$  (equivalent to a  $\pi/12$  tip angle), recycle delays of 2 s, and signal averaging of 1000 acquisitions. MAS NMR data were processed using commercial software, without additional apodization and referenced to aqueous aluminum nitrate at 0.0 ppm. A weak background signal from the zirconia MAS rotors was detected by  $^{27}\text{Al}$  MAS NMR of an empty rotor and subsequently subtracted from the MAS NMR

data of the glass samples. This signal, at approximately 16 ppm, is clearly distinct from the Al peaks in the glasses, but nonetheless has been removed to ensure higher quantitative accuracy in the  $^{27}\text{Al}$  MAS NMR experiments.

$^{29}\text{Si}$  MAS NMR data were collected at 4.7 T (39.69 MHz resonance frequency) using a 5 mm MAS NMR probe. Powdered samples were packed into 5 mm zirconia rotors and all measurements were conducted using 5 kHz sample spinning. Measurements were made with signal averaging of 320 to 2200 acquisitions, using  $\pi/6$  pulse widths of 1.4  $\mu\text{s}$  and recycle delays of 90 s.  $^{29}\text{Si}$  spectra were processed without additional line broadening and referenced to tetramethylsilane at 0.0 ppm.

X-ray photoelectron (XPS; Thermo K-alpha; Thermo Fisher Scientific) spectroscopy was used to study the structural coordination of molybdenum (Mo 3d) and neodymium (Nd 3d and Nd 4d) in glasses. The glasses were fractured prior their analysis by XPS. All the spectra were deconvoluted in CASA XPS software using Gaussian-Lorentzian peak fitting after Shirley background subtraction.<sup>30</sup> The deconvolutions were carried out subject to the constraint of a constant full width half maxima (FWHM) for the same element. All photoelectron binding energies were referenced to adventitious C 1s contamination peaks at a binding energy of 285.0 eV.

### 3. Results

#### 3.1. Crystallinity in glasses

Figure 1 presents the images of melt-quenched samples in the system  $25 \text{ Na}_2\text{O} - 5 \text{ Al}_2\text{O}_3 - 10 \text{ B}_2\text{O}_3 - (60-x) \text{ SiO}_2 - x \text{ MoO}_3$  ( $x = 0 - 4$  mol. %), while Figure 2a presents their XRD data. Homogeneous, transparent and completely amorphous samples were obtained for compositions with  $x = 0$  and 0.5 mol. %. An increase in  $\text{MoO}_3$  content to 1 mol. % resulted in a white translucent

sample, while further increase in MoO<sub>3</sub> content to 1.5 mol. % yielded a completely white and opaque sample. These physical characteristics can be attributed to either of the following scenarios: (i) liquid-liquid phase separation, or (ii) volume crystallization in the studied glasses. The XRD data of sample x = 1 reveals the presence of slight crystallization of SiO<sub>2</sub> and  $\gamma$ -Na<sub>2</sub>MoO<sub>4</sub> (orthorhombic) phases in the glassy matrix, while Na<sub>2</sub>MoO<sub>4</sub> (cubic) joined the crystalline phase assemblage with increasing MoO<sub>3</sub> content to 1.5 mol. %. Increasing MoO<sub>3</sub> content to 2 mol. % resulted in a white-colored opaque glass-ceramic with a thin layer of white-colored salt deposited on its surface. The concentration and thickness of this salt layer increased with further increase in MoO<sub>3</sub> content from 2 – 4 mol. % as is evident from [Figure 1](#). The quantitative phase analysis by Rietveld – RIR analysis on XRD data ([Table 1](#)) reveals that the resulting glass-ceramics with x = 2 – 4 mol. % were mostly amorphous (97 – 99 wt. %), with crystalline phase assemblage comprising Na<sub>2</sub>MoO<sub>4</sub> and  $\gamma$ -Na<sub>2</sub>MoO<sub>4</sub>. The XRD data of the salt layer presented in [Figure 3a](#) depicts their highly crystalline nature (high intensity phase reflections) with their phase assemblage being dominated by cubic Na<sub>2</sub>MoO<sub>4</sub> followed by Na<sub>2</sub>(MoO<sub>4</sub>)(H<sub>2</sub>O)<sub>2</sub>. [Figure 4](#) shows the SEM image along with EDS elemental mapping of an interface between glass-ceramic and salt layer for sample Na-Mo-4. The salt layer showed a dendritic microstructure, rich in Na<sub>2</sub>O and MoO<sub>3</sub>, confirming the crystallization of sodium molybdate phases, while most of the SiO<sub>2</sub> and Al<sub>2</sub>O<sub>3</sub> were confined to the glassy matrix.

An equimolar substitution of Na<sub>2</sub>O by CaO in 12.5 Na<sub>2</sub>O – 12.5 CaO – 5 Al<sub>2</sub>O<sub>3</sub> – 10 B<sub>2</sub>O<sub>3</sub> – (60-y) SiO<sub>2</sub> – y MoO<sub>3</sub> (y = 0 – 4 mol. %), system resulted in homogeneous, transparent and amorphous samples for compositions with x varying between 0 – 1.5 mol. %, as is evident from XRD data presented in [Figure 2b](#). An increase in MoO<sub>3</sub> content to 2 mol. % yielded a white, translucent sample, while the sample turned completely opaque for y = 2.5 mol. % (like the trend

observed in Na-Mo-x series, [Figure 1](#)). Further increase in MoO<sub>3</sub> content to 3 and 4 mol. % led to formation of a white-colored salt layer on the surface glass-ceramic samples. The resulting glass-ceramics were mostly amorphous (~96 wt. %) ([Table 1](#)) with small fractions of CaMoO<sub>4</sub> as the only crystalline phase, as shown in [Figure 2b](#). The XRD analysis ([Figure 3b](#)) of the salt layer formed on the surface of these samples shows the crystallization of CaMoO<sub>4</sub> as the dominant phase, followed by cubic Na<sub>2</sub>MoO<sub>4</sub>, Na<sub>2</sub>MoO<sub>4</sub>•2H<sub>2</sub>O and Na<sub>2</sub>Mo<sub>2</sub>O<sub>7</sub> as secondary phases. [Figure 5](#) shows the SEM image along with EDS elemental mapping of an interface between glass-ceramic and salt layer for sample Ca-Mo-4. The salt layer shows two distinct types of microstructures. One is rich in Na and Mo, suggesting sodium molybdate phases, while the other contains Ca and Mo, suggesting calcium molybdate phases. The glass-ceramic part of the sample comprises calcium- and molybdenum-rich crystalline inclusions embedded in aluminoborosilicate glass matrix.

Incorporating 5 mol. % Nd<sub>2</sub>O<sub>3</sub> at the expense of SiO<sub>2</sub> in 12.5 Na<sub>2</sub>O – 12.5 CaO – 5 Al<sub>2</sub>O<sub>3</sub> – 5 Nd<sub>2</sub>O<sub>3</sub> – 10 B<sub>2</sub>O<sub>3</sub> – (55-z) SiO<sub>2</sub> – z MoO<sub>3</sub> (z = 0 – 8 mol. %) had a significant impact on solubility of molybdate ions in the glass structure, as completely transparent and amorphous samples were obtained from compositions with z varying between 0 – 3 mol. % ([Figure 2c](#), and [Figure 6](#)). An increase in MoO<sub>3</sub> content to 3.5 mol. % resulted in a purple, translucent sample. However, its physical appearance was different from that observed for samples Na-Mo-1.5 or Ca-Mo-2 ([Figure 1](#)), as shown in [Figure 6](#). The XRD data shows the presence of low intensity phase reflections corresponding to crystallization of CaMoO<sub>4</sub> ([Figure 2c](#)). Increasing MoO<sub>3</sub> to 4 and 5 mol. % yielded opaque, volume crystallized glass-ceramics ([Figure 6](#)) with CaMoO<sub>4</sub> as the only crystalline phase. Further increase in MoO<sub>3</sub> to 6 mol. % resulted in formation of a faint dendritic pattern on the surface of glass-ceramic sample which became prominent with increasing MoO<sub>3</sub> content to 8 mol. %. The amount of residual glassy phase varied between 86 – 97 wt. % and

decreased with increasing MoO<sub>3</sub> content in these samples, remaining ~86 wt. % for the highest MoO<sub>3</sub> level tested (Table 1). While the XRD data of the glass-ceramic samples demonstrated the presence of CaMoO<sub>4</sub> as the only crystalline phase in these materials (as is evident from Figure 2c), the SEM imaging followed by EDS elemental mapping of these glass-ceramics (Figure 7) reveal the presence of three different microstructures – (1) a dendritic microstructure, rich in calcium, neodymium and molybdenum, spread across the surface of glass-ceramic in long chains; (2) a XRD amorphous microstructure rich in sodium and molybdenum, and (3) an amorphous phase rich in silica, alumina, and neodymium with small concentrations of sodium and calcium (being used to charge compensate AlO<sub>4</sub> (and possibly some BO<sub>4</sub>) units. The dendritic microstructure rich in Ca, Mo, and Nd (region 1) in Figure 7 corresponds to CaMoO<sub>4</sub> crystals as neodymium is known to incorporate in CaMoO<sub>4</sub> crystal structure as has been shown by Wang et al.<sup>31</sup> using micro laser induced breakdown spectroscopy. The microstructural organization of these materials suggest that the crystalline phase assemblage of resultant glass-ceramic (upon heat treatment) is expected to contain some volumetric CaMoO<sub>4</sub>, with Na<sub>2</sub>MoO<sub>4</sub> and a calcium-neodymium-rich phase on the surface. The EPMA results on RE-Mo-6 and RE-Mo-8 results (presented in Figure S1-S9) are in good agreement with the SEM-EDS results where the small white colored crystalline inclusions found in the bulk of the polished sample are rich in calcium, molybdenum and neodymium, while the glassy phase is rich in calcium, neodymium, aluminum and silicon. We could not confirm the presence or absence of phase separation in these samples due to difficulty with detection of boron in the presence of molybdenum. This problem has also been highlighted by Chouard et al.<sup>21</sup> The quantification of boron in molybdenum containing samples by EPMA is a known challenge<sup>32</sup> as B K<sub>α</sub> X-ray has an energy of 183.3 eV, but might shift slightly due to its bonding with Mo. This X-ray line energy is very close to the Mo M<sub>ζ</sub> line

that is at 192.6 eV. In addition, the K-shell absorption edge of boron is at 188 eV, just below the Mo  $M_{\zeta}$  line. Apart from that, a thin white colored salt layer was formed on the surface of glass-ceramic samples when MoO<sub>3</sub> content varied between 6 – 8 mol. %. The XRD analysis of this salt layer revealed the formation of CaMoO<sub>4</sub> as the dominant phase, followed by sodium molybdate based secondary phases – cubic Na<sub>2</sub>MoO<sub>4</sub>, and Na<sub>2</sub>MoO<sub>4</sub>•2H<sub>2</sub>O (Figure 3c).

Table 2 presents the liquidus temperature ( $T_L$ ) values of glasses from series RE-Mo-z (where, z varies between 0 – 3 mol.%) along with the first crystalline phase that forms in the melt at that temperature. The liquidus temperature of all the studied glasses varies between 1305 – 1330 °C and decreases from 1330 °C to 1305 °C with increasing MoO<sub>3</sub> concentration in glasses from 0 to 2 mol.%. However, with increase in MoO<sub>3</sub> concentration to 3 mol.%, the  $T_L$  again increases to  $1331.7 \pm 2.9$  °C. According to the XRD analysis (not shown), the composition of crystal formed at liquidus in all the rare-earth containing glasses Ca<sub>2</sub>Nd<sub>8</sub>(SiO<sub>4</sub>)<sub>6</sub>O<sub>2</sub>.

### 3.2. Solubility and retention of MoO<sub>3</sub> in glasses

Figure 8 presents the quantitative ICP-OES results demonstrating the target versus experimentally measured incorporation of MoO<sub>3</sub> in the studied glass systems. The data presented in Figure 8 for all the investigated glass systems can be divided into two parts: (i) a linear curve indicating all targeted MoO<sub>3</sub> is either dissolved in the glass or in crystals within the analyzed glass/glass-ceramic sample, which is denoted “apparent solubility,” (ii) a plateau (parallel to x – axis) representing the retention limit of MoO<sub>3</sub> in the samples, the excess of which partitioned to a salt phase that was washed off prior to chemical analysis, which is denoted “retention limit.” To distinguish between “true” and apparent solubility of Mo, the presence of crystals must be assessed (see below). For samples in Na-Mo-x series, the “true” solubility limit of MoO<sub>3</sub> may be defined as



~0.5 mol. % (1.12 wt.%), as further increase in molybdenum concentration resulted in the formation of crystalline inclusions of  $\text{Na}_2\text{MoO}_4$  in the glassy matrix. On the other hand, the retention limit of  $\text{MoO}_3$  in this system may be defined as 2 mol. % (4.41 wt.%), as higher concentrations of  $\text{MoO}_3$  could not be incorporated in the glass/glass-ceramic system, instead resulting in the formation of alkali molybdate rich crystalline salt on the surface of glass-ceramic which was removed prior to chemical analysis by ICP-OES.

An equimolar substitution of  $\text{Na}_2\text{O}$  by  $\text{CaO}$  (series Ca-Mo-y) led to an increase in  $\text{MoO}_3$  “true” solubility and retention limits to ~1.5 mol. % (3.37 wt. %) and 2.82 mol. % (6.22 wt. %), respectively. As has been discussed in Section 3.1, white colored crystalline salt rich in alkali and alkaline-earth molybdates was found on the surface of glass-ceramic Ca-Mo-3, thus, demonstrating that the retention limit of  $\text{MoO}_3$  in this glass/glass-ceramic system has been achieved or exceeded.

The partial substitution of 5 mol. %  $\text{Nd}_2\text{O}_3$  for  $\text{SiO}_2$  in the glass system had substantial impact on  $\text{MoO}_3$  solubility and retention limits. The  $\text{MoO}_3$  “true” solubility limit in the system RE-Mo-z increased to ~3 mol. % (5.45 wt. %) in comparison to ~1.5 mol. % for Ca-Mo-y glass system. Further increase in  $\text{MoO}_3$  concentration resulted in formation of  $\text{CaMoO}_4$  crystalline inclusions in the RE-Mo-z samples. The retention limit of  $\text{Nd}_2\text{O}_3$ -containing system increased to 6.7 mol. % (11.71 wt. %), as analyzed by ICP-OES data. This is interesting, because although salt formation was observed on the surface of samples with  $\text{MoO}_3 \geq 6$  mol. %, suggesting that retention limit for this composition has been achieved or exceeded, 6.7 mol. %  $\text{MoO}_3$  was still incorporated (retained) in these samples. The plausible explanation for this behavior has been presented in the discussion section.

### 3.3. Structure of glasses

#### 3.3.1. $^{11}\text{B}$ , $^{23}\text{Na}$ and $^{27}\text{Al}$ MAS NMR

Figure 9 presents the  $^{11}\text{B}$  MAS NMR spectra of glasses from Na-Mo-x series (Figure 9a) where x varies between 0 – 1 mol. %, and Ca-Mo-y, where y varies between 0 – 2 mol. % (Figure 9b). The  $^{11}\text{B}$  MAS NMR spectra of all the glasses shows two main features, a broad peak associated with  $\text{BO}_3$  ( $\text{B}^{\text{III}}$ ) units centered at ~13 ppm and a peak at ~ -1.6 ppm attributed to  $\text{BO}_4$  ( $\text{B}^{\text{IV}}$ ) units.<sup>37-</sup>  
<sup>39</sup> The deconvolution of MAS NMR spectra of these glasses reveal that  $\text{Na}_2\text{O}/\text{CaO}$  ratio had a significant impact on their borate speciation as the fraction of  $\text{N}_4$  units in Ca-Mo-y glasses ( $\text{N}_4 = 48 - 49\%$ ) was considerably lower than Na-Mo-x glasses ( $\text{N}_4 = 70 - 71\%$   $\text{N}_4$  units). The decrease of  $\text{B}^{\text{IV}}$  units with substitution of sodium by calcium demonstrates that the charge compensation of tetrahedral boron units is favored by sodium ions. The analysis of  $^{23}\text{Na}$  MAS NMR spectra from these glasses corroborated the  $^{11}\text{B}$  MAS NMR results, as the isotropic chemical shift for  $^{23}\text{Na}$  moves to high shielding, and the quadrupolar coupling constant ( $C_Q$ ) gets smaller with the partial substitution of  $\text{Na}_2\text{O}$  by  $\text{CaO}$ , as shown in Figure 10. These observations suggest the change in the structural role of sodium from modifier to charge compensator when  $\text{CaO}$  is added. Similar results on alkali/alkaline-earth aluminoborosilicate glasses have been published by Quintas et al.<sup>40</sup> In accordance with the literature on this subject, there is only modest impact of molybdenum incorporation on sodium or borate speciation in the studied glasses,<sup>4, 12</sup> with a continuous change in  $^{23}\text{Na}$  NMR parameters with increasing  $\text{MoO}_3$  (Figure 10).

Figure 11 shows a comparison of  $^{27}\text{Al}$  MAS NMR spectra recorded for the Na-Mo-x (Figure 11a) and Ca-Mo-y (Figure 11b) glass series. The spectra show nearly symmetric peaks located around 60 ppm in both series, which reflects the tetrahedral coordination ( $\text{Al}^{\text{IV}}$ ) of

aluminum atoms in aluminosilicates.<sup>41-44</sup> This confirms adequate charge-balancing of Al tetrahedra, as expected for these highly peralkaline glass compositions.

### 3.3.2. XPS analysis

XPS was used to study the structural coordination of molybdenum and neodymium in the rare-earth containing glasses (RE-Mo-z). Figure 12 presents the Mo 3d (Figure 12a) and Nd 3d (Figure 12b) XPS spectra of glass RE-Mo-3. The observed features in the XPS spectra for the RE-Mo-3 glass are representative of all the Nd<sub>2</sub>O<sub>3</sub>-containing glass samples discussed in this study. Table 2 presents the binding energies (peak positions from XPS data) for Mo 3d<sub>3/2</sub>, Mo 3d<sub>5/2</sub>, Nd 3d<sub>3/2</sub>, Nd 3d<sub>5/2</sub> and Nd 4d spin states as observed in the present study, along with a comparison with their values reported in literature.<sup>15, 45, 46</sup> The Mo 3d XPS spectra shows two main peaks at 232 eV and 235 eV corresponding to Mo<sup>6+</sup> 3d<sub>5/2</sub> and 3d<sub>3/2</sub> spin states, respectively. This confirms the assertion of Mo being mainly in a hexavalent oxidation state in the studied glasses. According to Farges et al.,<sup>47</sup> Mo is present primarily as [Mo(VI)O<sub>4</sub><sup>2-</sup>] species in most of the silicate and aluminosilicate glass compositions synthesized at f(O<sub>2</sub>) values ranging from 1 atm to 10<sup>-12</sup> atm. Regarding the structural coordination of neodymium, the Nd 3d spectra exhibit two main peaks at 983 eV and 1005 eV, corresponding to Nd 3d<sub>5/2</sub> and Nd 3d<sub>3/2</sub>, respectively, while the Nd 4d spectra exhibits a single broad peak at 121 eV. According to the literature,<sup>45, 46</sup> these binding energies are typically found for neodymium environments in Nd<sub>2</sub>O<sub>3</sub> and Nd(OH)<sub>3</sub>, i.e. Nd<sup>3+</sup>.

## 4. Discussion

### 4.1. Solubility of molybdate ions in rare-earth free aluminoborosilicate glasses

The coordination of MoO<sub>4</sub><sup>2-</sup> ions in a borosilicate or aluminoborosilicate glass is highly dependent on its homogeneous vs. heterogeneous nature. According to available literature on his

topic, in a homogeneous borosilicate glass, molybdate ions are located in the depolymerized regions of the glass structure (i.e., non-bridging oxygen (NBO)-rich regions) containing alkali and alkaline-earth cations to compensate their negative charge.<sup>48</sup> On the other hand, in a phase separated borosilicate glass, incorporation of even small concentration (~1 mol. % MoO<sub>3</sub>) of molybdate ions are known to further promote phase separation, resulting in segregation of alkali-borate-rich amorphous domains from a silica-rich matrix.<sup>19</sup> An increase in MoO<sub>3</sub> concentration in this case leads to a decrease in SiO<sub>2</sub> content in alkali-borate-rich regions and an increased volume fraction of a SiO<sub>2</sub>-rich phase, and most of the molybdate ions coordinate into the alkali-borate-rich region.<sup>19</sup> Similar structural behavior of molybdate ions can be expected in aluminoborosilicate glasses based on their homogeneous or heterogeneous nature. However, most of the literature pertaining to molybdenum incorporation in aluminoborosilicate glasses relates to homogeneous parent glasses, where molybdate ions are not directly linked to the aluminoborosilicate glass network but rather located within alkali and alkaline-earth domains in the glass.<sup>12</sup> This explanation is in good agreement with the results obtained in the present study for glasses in Na-Mo-x and Ca-Mo-y series. The structural position of molybdate ions in the depolymerized regions of glass (rich in NBOs), and being charge compensated by Na<sup>+</sup> in Na-Mo-x and both Na<sup>+</sup> and Ca<sup>2+</sup> in Ca-Mo-y glasses, explains the crystallization of Na<sub>2</sub>MoO<sub>4</sub> and CaMoO<sub>4</sub> phases in the respective series of glasses. Since MoO<sub>3</sub> incorporation in the studied glasses did not affect their boron and aluminum speciation, it is highly likely that sodium and calcium are being pulled from the silica matrix to form Na<sub>2</sub>MoO<sub>4</sub> or CaMoO<sub>4</sub> phases, thus leading to repolymerization of the silicate network. Interestingly, <sup>29</sup>Si MAS NMR of glasses in Na-Mo-x series (Figure S10) does not exhibit any significant shift as a function of MoO<sub>3</sub> content. However, this does not imply absence of repolymerization in the silicate network, as insignificant shifts in <sup>29</sup>Si MAS NMR spectra can be due

to small or undetectable change in the silicate network owing to the low concentration of MoO<sub>3</sub>, and additional complications due to Si/Al mixing in the glass network.

The drastic change in boron speciation, i.e., the substantial reduction in the fraction of boron in four-fold coordination due to introduction of CaO (at the expense of Na<sub>2</sub>O), may be explained based on the higher ionic field strength of Ca<sup>2+</sup> compared to Na<sup>+</sup>. Higher field strength cations significantly favor the formation of NBO, lowering the degree of preference in formation of B<sup>IV</sup> over NBO.<sup>49</sup> For detailed explanations, readers are referred the following literature.<sup>40, 49, 50</sup> The consequences of this difference in modifier behavior (e.g., N<sub>4</sub>) is such that the Ca<sup>2+</sup> is then more associated with silicon, forming a much higher proportion of Si-NBO than the analogous Na-bearing glasses. As discussed above, incorporation of MoO<sub>3</sub> in Na<sub>2</sub>O – CaO – Al<sub>2</sub>O<sub>3</sub> – B<sub>2</sub>O<sub>3</sub> – SiO<sub>2</sub> glass will result in formation of alkali and alkaline-earth molybdate species, first as associated moieties in the glass and ultimately as precipitated crystals. However, the formation of CaMoO<sub>4</sub> (over Na<sub>2</sub>MoO<sub>4</sub>) as the preferential crystalline phase in these glass-ceramics may be attributed to the unavailability of Na<sup>+</sup> to associate with (MoO<sub>4</sub>)<sup>2-</sup>, because the majority of sodium is being used to charge compensate for B<sup>IV</sup> and Al<sup>IV</sup> units, as reflected in the B and Al coordination numbers and the <sup>23</sup>Na NMR data.<sup>4</sup> Further, the higher solubility of molybdate ions in Na<sub>2</sub>O – CaO – Al<sub>2</sub>O<sub>3</sub> – B<sub>2</sub>O<sub>3</sub> – SiO<sub>2</sub> glass system, in comparison to Na<sub>2</sub>O – Al<sub>2</sub>O<sub>3</sub> – B<sub>2</sub>O<sub>3</sub> – SiO<sub>2</sub> system, may be attributed to the slower tendency of the former towards devitrification due to the higher activation energy of crystallization of CaMoO<sub>4</sub> (~50 – 60 kcal/mole) versus Na<sub>2</sub>MoO<sub>4</sub> (~28 kcal/mole).<sup>51</sup>

#### **4.2 Impact of Nd<sub>2</sub>O<sub>3</sub> on MoO<sub>3</sub> solubility in aluminoborosilicate glasses**

Before we discuss the impact of Nd<sub>2</sub>O<sub>3</sub> on the solubility of MoO<sub>3</sub> in the aluminoborosilicate glasses under investigation, it is important to understand the structural role of

$\text{Nd}_2\text{O}_3$  in these glasses as it has direct implications on the solubility of  $\text{MoO}_3$ . The structural coordination of rare-earth cations in alkali/alkaline-earth aluminoborosilicate glasses has been studied in detail primarily by researchers from two countries – USA,<sup>33, 34, 52-59</sup> and France<sup>40, 60-65</sup> owing to their high relevance in the field of nuclear waste immobilization. Based on the investigated compositional chemistries, there exist two different opinions about the coordination of rare-earth cations in these glasses. According to the U.S. scientists (hereafter referred as Li et al.), who studied a wide array of glass compositions in  $\text{Na}_2\text{O}-\text{Al}_2\text{O}_3-\text{B}_2\text{O}_3-\text{SiO}_2$  based per-alkaline and per-aluminous systems, the role of rare-earth cation in a per-alkaline ( $\text{Na}/\text{Al}>1$ ) glass (most nuclear waste glasses are per-alkaline) is decided by the ratio of  $\text{Na}_2\text{O}_{\text{ex}}/\text{B}_2\text{O}_3$ , where  $\text{Na}_2\text{O}_{\text{ex}} = [\text{Na}_2\text{O}] - [\text{Al}_2\text{O}_3]$ .<sup>33</sup> It has been suggested that if  $\text{Na}_2\text{O}_{\text{ex}}/\text{B}_2\text{O}_3 < 0.5$ , the baseline aluminoborosilicate glass is heterogeneous (phase separated), while glasses with  $\text{Na}_2\text{O}_{\text{ex}}/\text{B}_2\text{O}_3 > 0.5$  are homogeneous in nature. In case of phase separated glass ( $\text{Na}_2\text{O}_{\text{ex}}/\text{B}_2\text{O}_3 < 0.5$ ), rare-earth cation is mostly incorporated in the borate portion of the structural phase.<sup>33</sup>

The rare-earth free per-alkaline glasses with  $\text{Na}_2\text{O}_{\text{ex}}/\text{B}_2\text{O}_3 > 0.5$ , for example,  $60\text{SiO}_2 \cdot 15\text{B}_2\text{O}_3 \cdot 20\text{Na}_2\text{O} \cdot 5\text{Al}_2\text{O}_3$  (mol.%),<sup>52, 58</sup> have been shown to be homogeneous. The incorporation of rare-earth cations in these glasses phase separates the homogeneous aluminoborosilicate glass into borate- and aluminosilicate-rich zones where the rare-earth cations preferentially enter the borate-rich phase forming a double chain structure similar to rare-earth metaborate. Once the concentration of rare-earth cations in the glass exceeds its solubility limit in the borate phase, the rare-earth cations are incorporated in the aluminosilicate phase as some kind of “cluster”. This mechanism has been proven for  $\text{Gd}_2\text{O}_3$  and  $\text{Nd}_2\text{O}_3$  containing aluminoborosilicate glasses by transmission electron microscopy (TEM) and multi-spectroscopic

techniques, including electron energy loss spectroscopy (EELS) and optical spectroscopy.<sup>33, 34, 53, 54, 56</sup>

In case of studies performed by French scientists (hereafter referred as Caurant et al.) on this subject, majority of the experimental research has employed the following two baseline compositions (mol.%): 16.56 Na<sub>2</sub>O – 8.28 CaO – 5.32 Al<sub>2</sub>O<sub>3</sub> – 10.65 B<sub>2</sub>O<sub>3</sub> – 59.17 SiO<sub>2</sub><sup>21, 62</sup> and 14.41 Na<sub>2</sub>O – 6.33 CaO – 3.05 Al<sub>2</sub>O<sub>3</sub> – 8.94 B<sub>2</sub>O<sub>3</sub> – 1.90 ZrO<sub>2</sub> – 3.56 RE<sub>2</sub>O<sub>3</sub> – 61.81 SiO<sub>2</sub> (RE: Rare-earth).<sup>40, 63, 65, 66</sup> Considering the Na<sub>2</sub>O<sub>ex</sub>/B<sub>2</sub>O<sub>3</sub> criteria as proposed by Li et al.,<sup>33</sup> both the baseline compositions (when rare-earth free) should be homogeneous in nature. While similar results have been published by Caurant et al.,<sup>40, 60, 62, 63</sup> they tend to disagree with Li et al.<sup>33, 52, 58</sup> with regard to the induction of phase separation by rare-earth cations in a homogeneous aluminoborosilicate glass. According to Caurant et al.,<sup>21, 62</sup> Nd<sup>3+</sup> act as network modifier in aluminoborosilicate glasses where they remain located in the depolymerized silicate regions of the glassy network and thanks to their high ionic field strength, they impose their local environment composed of 6 – 8 NBOs. Nevertheless, in order to insure locally the configuration electroneutrality, a fraction of the lower field strength modifier cations present in the glass composition such as alkali and alkaline-earth cations are located in the second coordination sphere of the Nd<sup>3+</sup> cations. Further it has been reported that glass-in-glass phase separation in rare-earth containing glasses is detected when CaO/Na<sub>2</sub>O >1, while the glasses with CaO/Na<sub>2</sub>O < 1 are homogeneous in nature.<sup>40</sup>

In order to clarify the contradiction between the results from two research groups, Caurant et al.<sup>67</sup> conducted an extensive study investigating two different series of per-alkaline glass compositions (first with Na<sub>2</sub>O<sub>ex</sub>/B<sub>2</sub>O<sub>3</sub> < 0.5 and second with Na<sub>2</sub>O<sub>ex</sub>/B<sub>2</sub>O<sub>3</sub> > 0.5) derived from 14.41 Na<sub>2</sub>O – 6.33 CaO – 3.05 Al<sub>2</sub>O<sub>3</sub> – 8.94 B<sub>2</sub>O<sub>3</sub> – 1.90 ZrO<sub>2</sub> – 3.56 Nd<sub>2</sub>O<sub>3</sub> – 61.81 SiO<sub>2</sub> as the

base composition. In accordance with Li et al.,<sup>33</sup> they reported that the key chemical parameter governing the overall structural organization in these glasses is the  $\text{Na}_2\text{O}_{\text{ex}}/\text{B}_2\text{O}_3$  ratio, where  $\text{Na}_2\text{O}_{\text{ex}} = [\text{Na}_2\text{O}] - [\text{Al}_2\text{O}_3] - [\text{ZrO}_2]$ , and the high field strength cations, for example,  $\text{Ca}^{2+}$  and  $\text{Nd}^{3+}$ , only interfere on the second order of their structural organization, inducing more disorder in it. Based on  $\text{Nd}^{3+}$  optical absorption spectroscopy and  $\text{Nd}^{3+}$  L3-edge X-ray absorption spectroscopy, Caurant et al.,<sup>67</sup> indicated towards the possible formation of  $\text{Nd}^{3+}$ ,  $\text{Ca}^{2+}$ , NBOs and  $\text{BO}_4^-$  rich areas in the glasses with  $\text{Na}_2\text{O}_{\text{ex}}/\text{B}_2\text{O}_3 > 0.5$ . They attributed the presence of borate units around  $\text{Nd}^{3+}$  ions in the glass structure as a reason for slower tendency towards apatite crystallization (upon slow cooling of glass melt) with increasing  $\text{B}_2\text{O}_3$  concentration. However, they still reported the glasses to be “sufficiently homogeneous in terms of Si/B mixing” to undergo crystallization of the Nd-rich silicate apatite phase by slow cooling the melt. In case of  $\text{B}_2\text{O}_3$  rich glasses, i.e.  $\text{Na}_2\text{O}_{\text{ex}}/\text{B}_2\text{O}_3 < 0.5$ , they reported the presence of glass-in-glass phase separation where formation of Na-rich or Nd-metaborate phase was confirmed.

In the present study,  $\text{Na}_2\text{O}_{\text{ex}}/\text{B}_2\text{O}_3 > 0.5$  for the rare-earth free glass Ca-Mo-0. Therefore, in accordance with the existing literature on this topic, this glass should be homogeneous in nature where sodium is mainly acting as a charge compensator for  $\text{AlO}_4^-$  and  $\text{BO}_4^-$  units. This assertion is supported by the  $^{23}\text{Na}$ ,  $^{27}\text{Al}$  and  $^{11}\text{B}$  MAS-NMR results of Ca-Mo-y glass series as discussed in the results section. Further, when  $\text{Nd}_2\text{O}_3$  is added to the glass Ca-Mo-0 (resulting in RE-Mo-0), each  $\text{Nd}^{3+}$  brings 3 NBOs, while it needs 6 – 8 NBOs to fulfill its coordination in order to be homogeneously incorporated in the glass structure.<sup>67</sup> Therefore, for each mole of  $\text{Nd}_2\text{O}_3$ , 3 to 5 moles of  $(\text{Na}_2\text{O} + \text{CaO})$  will be required to homogeneously incorporate  $\text{Nd}^{3+}$  ions within the fully charge-compensated polyhedral. Since majority of sodium is acting as charge compensator for four coordinated aluminum and boron,  $\text{Nd}^{3+}$  will tend to coordinate with NBOs being generated



by  $\text{Ca}^{2+}$  in order to fulfill its coordination shell. However, there is not enough concentration of network modifiers for the required job. In this scenario,  $\text{Nd}^{3+}$  can be incorporated in the glass through following two possible mechanisms: (i) they can form clusters where they can share their own NBOs, or (ii) they can contribute to the charge compensation of  $\text{BO}_4$  units (since  $\text{AlO}_4$  units are completely charge balanced by  $\text{Na}^+$ ). According to Caurant et al.<sup>67</sup> both the mechanisms are possible, where, a part of  $\text{Nd}^{3+}$  charge compensates boron to form  $\text{BO}_4$  units, while the remaining form clusters, thus distributing itself in borosilicate phase of the glass. Although they do not agree with the hypothesis of phase separation in rare-earth containing glasses as proposed by Li et al.<sup>53</sup>, their results from reference<sup>67</sup> point in the same direction where  $\text{Nd}^{3+}$  are distributed in the borosilicate matrix, preferentially being associated with tetrahedral borate moieties followed by clustering in silicate part.

Regarding the impact of  $\text{Nd}_2\text{O}_3$  on the solubility of  $\text{MoO}_3$  in aluminoborosilicate glasses, it has been proposed that it is the close relationship between  $\text{Nd}^{3+}$  and  $[\text{MoO}_4]^{2-}$  tetrahedral entities in the depolymerized region of the glassy network that is at the origin of the increase of molybdenum solubility and of the disappearance of phase separation and crystallization of molybdate phases.<sup>20, 21, 68</sup> According to the proposed hypothesis, the presence of neodymium has a “dispersing effect” on the  $[\text{MoO}_4]^{2-}$  units in the glass which avoids their clustering and crystallization of molybdate phases.<sup>21</sup> While the proposed hypothesis tends to explain the suppression in crystallization of molybdate phases, it contradicts the results from the same research group presented in reference<sup>67</sup> regarding structural coordination of  $\text{Nd}^{3+}$  in aluminoborosilicate glasses as discussed above.

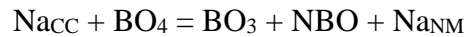
In our opinion,  $\text{MoO}_4^{2-}$  when incorporated in aluminoborosilicate glass associates itself with  $\text{Nd}^{3+}$ ,  $\text{Ca}^{2+}$ , NBOs and  $\text{BO}_4^-$  rich regions. This is in agreement with the TEM studies on molybdenum containing borosilicate glasses reported by Kawamoto et al.,<sup>19</sup> where it has been

shown that molybdate ions prefer to enter the borate-rich phase of a phase separated borosilicate glass (discussed above). While we could not ascertain the possibility of phase separation in rare-earth aluminoborosilicate glass due to poor detection of boron in both SEM-EDS, and EPMA, this does not negate the possibility of phase separation in glasses upon addition of molybdenum oxide. This argument is based on the fact that both Li et al.<sup>33</sup> and Caurant et al.<sup>67</sup> have discussed the formation of rare-earth rich borate regions in aluminoborosilicate glasses, although the latter describes their glasses to be “sufficiently homogeneous” when  $\text{Na}_2\text{O}_{\text{ex}}/\text{B}_2\text{O}_3 > 0.5$ . Therefore, it is highly likely that once incorporated into the borate phase,  $\text{MoO}_4^{2-}$  ions coordinate with the rare-earth- borate phase to form a rare-earth-molybdate-borate glassy phase. The formation of this  $\text{Nd}_2\text{O}_3\text{--MoO}_3\text{--B}_2\text{O}_3$  glassy phase resulted in higher solubility of molybdate ions in the studied glasses. This assertion is supported by the fact that stable glass-forming regions in the  $\text{La}_2\text{O}_3\text{--MoO}_3\text{--B}_2\text{O}_3$  and  $\text{Nd}_2\text{O}_3\text{--MoO}_3\text{--B}_2\text{O}_3$  systems have been reported by Aleksandrov et al.<sup>35, 36</sup> According to the literature, molybdenum exists as  $\text{MoO}_4^{2-}$  species in the  $\text{Nd}_2\text{O}_3\text{--MoO}_3\text{--B}_2\text{O}_3$  glassy system. Neutron diffraction and reverse Monte Carlo (RMC) simulations show an existence of pronounced intermediate – range ordering through  $\text{MoO}_4\text{--BO}_4$  and  $\text{MoO}_4\text{--BO}_3$  linkages.<sup>69</sup>

Our hypothesis is also supported by the crystallization of Nd-rich  $\text{CaMoO}_4$  phase in RE-Mo-z glasses with  $\text{MoO}_3 \geq 3.5$  mol. % (Figure 7). An increase in  $\text{MoO}_3 \geq 3.5$  mol.% likely exceeded the concentration of molybdate ions that could be accommodated in the  $\text{Nd}_2\text{O}_3\text{--MoO}_3\text{--B}_2\text{O}_3$  glassy structure, thus leading to crystallization of  $\text{CaMoO}_4$ . The proposed hypothesis also gains support from the crystallization of  $\text{Ca}_{2.2}\text{Nd}_{7.8}(\text{SiO}_4)_6\text{O}_{1.9}$  based apatite phase at liquidus temperature in rare-earth containing glasses. This may be attributed to the structural re-arrangement between silicate component of glass and neodymium clusters at high temperatures resulting in crystallization of apatite.

### 4.3 Salt formation in molybdenum-rich glass melts

While the glass-ceramics from the Ca-Mo-y and RE-Mo-z systems exhibited the crystallization of CaMoO<sub>4</sub> phase in their glassy matrix, the white salt phase formed in MoO<sub>3</sub>-rich melts contained both CaMoO<sub>4</sub> and polymorphs of Na<sub>2</sub>MoO<sub>4</sub>. The chemical difference between the nature of crystalline molybdates, which may form in the high temperature melt versus the cooled glass-ceramic, may be explained based on temperature-induced coordination changes of boron, leading to the modifications in the activity of alkali/alkaline-earth cations, which act as either charge compensators or network modifiers. According to previous studies,<sup>12, 38, 70, 71</sup> boron partially changes from tetrahedral to triangular coordination with increasing temperature in borosilicate glasses. Therefore, an increase in the activity (i.e., concentration) of network modifying alkali cations can be expected at an increased temperature, according to the reaction:



where, Na<sub>ACC</sub> and Na<sub>NM</sub> refer to charge compensating and network modifier roles of Na, respectively. Thus, under oxidizing conditions, alkali molybdates will form in the molten stage due to higher availability of alkali cations in the presence of 3-coordinated boron. On the other hand, the partial transformation of boron from 3- to 4- coordination during cooling of the glass will increase the proportion of Na cations involved in charge compensation of boron. Consequentially, there will be no more Na<sup>+</sup> to charge compensate molybdate groups, and Ca<sup>2+</sup> ions will be required to fulfill this role.

## 5. Conclusions

An attempt has been made to understand the compositional and structural dependence of molybdate ions in aluminoborosilicate based model nuclear waste glasses. The higher solubility

of MoO<sub>3</sub> in Na-Ca-Al-B-Si-O glass in comparison to Na-Al-B-Si-O has been explained on the basis of unavailability of sodium ions to charge compensate MoO<sub>4</sub><sup>2-</sup>, thus resulting in the charge compensation of latter by Ca<sup>2+</sup>. This leads to the crystallization of CaMoO<sub>4</sub> (over Na<sub>2</sub>MoO<sub>4</sub>) in calcium-containing aluminoborosilicate glasses. Since the activation energy of crystallization for CaMoO<sub>4</sub> is about double that of Na<sub>2</sub>MoO<sub>4</sub>, this results in higher solubility of MoO<sub>3</sub> in Na-Ca-Al-B-Si-O glass system. Further, the introduction of Nd<sub>2</sub>O<sub>3</sub> in the Na-Ca-Al-B-Si-O glass system increases the solubility of MoO<sub>3</sub> from 1.5 mol. % to 3 mol. %. This increase in MoO<sub>3</sub> solubility as a function of Nd<sub>2</sub>O<sub>3</sub> has been explained on the basis of three-step mechanism where in **Step 1, a fraction of rare-earth cations distributes themselves in the borate rich areas of glass while the remaining rare-earth cations cluster in the silicate/borosilicate region.** In Step 2, the MoO<sub>4</sub><sup>2-</sup> ions are incorporated into the rare-earth borate phase, thus forming a stable Nd-Mo-B-O glassy region. In Step 3, any further increase in MoO<sub>3</sub> concentration (in this case MoO<sub>3</sub> ≥ 3.5 mol. %) is likely to exceed the concentration of molybdate ions that could be accommodated in the Nd<sub>2</sub>O<sub>3</sub>-MoO<sub>3</sub>-B<sub>2</sub>O<sub>3</sub> glassy structure, thus leading to crystallization of Nd-rich CaMoO<sub>4</sub>.

### **Acknowledgements**

This research is being performed using funding received from the U.S. Department of Energy – Office of Nuclear Energy through the Nuclear Energy University Program under the award DE-NE0008431 and DE-NE0008597. Authors acknowledge the support of Corning Research & Development Corporation for ICP-OES and MAS-NMR measurements.

## References

1. Jin, T.; Kim, D.; Tucker, A. E.; Schweiger, M. J.; Kruger, A. A., Reactions during melting of low-activity waste glasses and their effects on the retention of rhenium as a surrogate for technetium-99. *Journal of Non-Crystalline Solids* **2015**, 425, 28-45.
2. McCloy, J. S.; Riley, B. J.; Goel, A.; Liezers, M.; Schweiger, M. J.; Rodriguez, C. P.; Hrma, P.; Kim, D.-S., Rhenium Solubility in Borosilicate Nuclear Waste Glass: Implications for the Processing and Immobilization of Technetium-99. *Environmental Science & Technology* **2012**, 46 (22), 12616-12622.
3. Darab, J. G.; Smith, P. A., Chemistry of Technetium and Rhenium Species during Low-Level Radioactive Waste Vitrification. *Chemistry of Materials* **1996**, 8 (5), 1004-1021.
4. Magnin, M.; Schuller, S.; Mercier, C.; Trebosc, J.; Caurant, D.; Majerus, O.; Angeli, F.; Charpentier, T., Modification of Molybdenum Structural Environment in Borosilicate Glasses with Increasing Content of Boron and Calcium Oxide by <sup>95</sup>Mo MAS NMR. *Journal of the American Ceramic Society* **2011**, 94 (12), 4274-4282.
5. Schuller, S.; Pinet, O.; Grandjean, A.; Blisson, T., Phase separation and crystallization of borosilicate glass enriched in MoO<sub>3</sub>, P<sub>2</sub>O<sub>5</sub>, ZrO<sub>2</sub>, CaO. *J. Non-Cryst. Solids* **2008**, 354 (2-9), 296-300.
6. Vienna, J. D.; Kim, D.-S.; Muller, I. S.; Piepel, G. F.; Kruger, A. A., Toward Understanding the Effect of Low-Activity Waste Glass Composition on Sulfur Solubility. *Journal of the American Ceramic Society* **2014**, 97 (10), 3135-3142.
7. Manara, D.; Grandjean, A.; Pinet, O.; Dussossoy, J. L.; Neuville, D. R., Sulfur behavior in silicate glasses and melts: Implications for sulfate incorporation in nuclear waste glasses as a function of alkali cation and V<sub>2</sub>O<sub>5</sub> content. *Journal of Non-Crystalline Solids* **2007**, 353 (1), 12-23.
8. Jantzen, C. M.; Imrich, K. J.; Pickett, J. B.; Brown, K. G., High Chrome Refractory Characterization: Part I. Impact of Melt Reduction/Oxidation on the Corrosion Mechanism. *International Journal of Applied Glass Science* **2015**, 6 (2), 137-157.
9. Crum, J.; Maio, V.; McCloy, J.; Scott, C.; Riley, B.; Benefiel, B.; Vienna, J.; Archibald, K.; Rodriguez, C.; Rutledge, V.; Zhu, Z. H.; Ryan, J.; Olszta, M., Cold crucible induction melter studies for making glass ceramic waste forms: A feasibility assessment. *J. Nucl. Mater.* **2014**, 444 (1-3), 481-492.
10. Crum, J. V.; Riley, B. J.; Turo, L. R.; Tang, M.; Kossoy, A. Glass-ceramic waste forms for combined fission products; Pacific Northwest National Laboratory: Richland, WA, 2011.
11. Nicoleau, E.; Schuller, S.; Angeli, F.; Charpentier, T.; Jollivet, P.; Le Gac, A.; Fournier, M.; Mesbah, A.; Vasconcelos, F., Phase separation and crystallization effects on the structure and durability of molybdenum borosilicate glass. *Journal of Non-Crystalline Solids* **2015**, 427, 120-133.
12. Calas, G.; Le Grand, M.; Galoisy, L.; Ghaleb, D., Structural role of molybdenum in nuclear glasses: an EXAFS study. *J. Nucl. Mater.* **2003**, 322 (1), 15-20.
13. Pinet, O.; Dussossoy, J. L.; David, C.; Fillet, C., Glass matrices for immobilizing nuclear waste containing molybdenum and phosphorus. *Journal of Nuclear Materials* **2008**, 377 (2), 307-312.
14. Hand, R. J.; Short, R. J.; Morgan, S.; Hyatt, N. C.; Mobus, G.; Lee, W. E., Molybdenum in glasses containing vitrified nuclear waste. *Glass Technol.* **2005**, 46 (2), 121-124.

15. Short, R. J.; Hand, R. J.; Hyatt, N. C.; Mobus, G., Environment and oxidation state of molybdenum in simulated high level nuclear waste glass compositions. *J. Nucl. Mater.* **2005**, 340 (2-3), 179-186.
16. Ishiguro, K.; Kawanishi, N.; Nagaki, H.; Naito, A. Chemical states of molybdenum in radioactive waste glass; Japan, 1982; pp 107-115.
17. Kawamura, K.; Ohuchi, J. In CHARACTERIZATION OF HIGHLY WASTE LOADED GLASS FOR HLW, 18th International Symposium on the Scientific Basis for Nuclear Waste Management, Kyoto, Japan, Oct 23-27; Kyoto, Japan, 1994; pp 87-93.
18. McKeown, D. A.; Gan, H.; Pegg, I. L., X-ray absorption and Raman spectroscopy studies of molybdenum environments in borosilicate waste glasses. *Journal of Nuclear Materials* **2017**.
19. Kawamoto, Y.; Clemens, K.; Tomozawa, M., EFFECTS OF MOO<sub>3</sub> ON PHASE-SEPARATION OF NA<sub>2</sub>O-B<sub>2</sub>O<sub>3</sub>-SIO<sub>2</sub> GLASSES. *Journal of the American Ceramic Society* **1981**, 64 (5), 292-296.
20. Chouard, N.; Caurant, D.; Majerus, O.; Guezi-Hasni, N.; Dussossoy, J. L.; Baddour-Hadjean, R.; Pereira-Ramos, J. P., Thermal stability of SiO<sub>2</sub>-B<sub>2</sub>O<sub>3</sub>-Al<sub>2</sub>O<sub>3</sub>-Na<sub>2</sub>O-CaO glasses with high Nd<sub>2</sub>O<sub>3</sub> and MoO<sub>3</sub> concentrations. *Journal of Alloys and Compounds* **2016**, 671, 84-99.
21. Chouard, N.; Caurant, D.; Majerus, O.; Dussossoy, J. L.; Ledieu, A.; Peugeot, S.; Baddour-Hadjean, R.; Pereira-Ramos, J. P., Effect of neodymium oxide on the solubility of MoO<sub>3</sub> in an aluminoborosilicate glass. *Journal of Non-Crystalline Solids* **2011**, 357 (14), 2752-2762.
22. Crum, J. V.; Billings, A. L.; Lang, J.; Marra, J. C.; Rodriguez, C.; Ryan, J. V.; Vienna, J. D., Baseline Glass Development for Combined Fission Products Waste Streams. US Department of Energy Report AFCI-WAST-WAST-MI-DV-2009 **2009**, 75.
23. Tan, S. H.; Ojovan, M. I.; Hyatt, N. C.; Hand, R. J., MoO<sub>3</sub> incorporation in magnesium aluminosilicate glasses. *Journal of Nuclear Materials* **2015**, 458, 335-342.
24. Balazs, G. B.; Russel, C., ELECTROCHEMICAL STUDIES OF THE CORROSION OF MOLYBDENUM ELECTRODES IN SODA-LIME GLASS MELTS. *Journal of Non-Crystalline Solids* **1988**, 105 (1-2), 1-6.
25. Kim, D.; Schweiger, M. J., Incorporation and distribution of rhenium in a borosilicate glass melt heat treated in a sealed ampoule. *Journal of Non-Crystalline Solids* **2013**, 379, 123-126.
26. Lee, W. E.; Ojovan, M. I.; Stennett, M. C.; Hyatt, N. C., Immobilisation of radioactive waste in glasses, glass composite materials and ceramics. *Advances in Applied Ceramics* **2006**, 105 (1), 3-12.
27. Konstantinou, K.; Sushko, P. V.; Duffy, D. M., Modelling the local atomic structure of molybdenum in nuclear waste glasses with ab initio molecular dynamics simulations. *Physical Chemistry Chemical Physics* **2016**, 18 (37), 26125-26132.
28. Massiot, D.; Fayon, F.; Capron, M.; King, I.; Le Calvé, S.; Alonso, B.; Durand, J. O.; Bujoli, B.; Gan, Z.; Hoatson, G., Modelling one-and two-dimensional solid-state NMR spectra. *Magnetic Resonance in Chemistry* **2002**, 40 (1), 70-76.
29. Massiot, D.; Bessada, C.; Coutures, J.; Taulelle, F., A quantitative study of <sup>27</sup>Al MAS NMR in crystalline YAG. *Journal of Magnetic Resonance (1969)* **1990**, 90 (2), 231-242.
30. Herrera-Gomez, A. The Peak-Shirley Background; Centro de Investigación y de Estudios Avanzados del Instituto Politécnico Nacional (CINVESTAV-IPN) Centro de Investigación y de Estudios Avanzados del Instituto Politécnico Nacional (CINVESTAV-IPN): Mexico, 2012.
31. Wang, X.; Motto-Ros, V.; Panczer, G.; De Ligny, D.; Yu, J.; Benoit, J. M.; Dussossoy, J. L.; Peugeot, S., Mapping of rare earth elements in nuclear waste glass-ceramic using micro laser-

- induced breakdown spectroscopy. *Spectrochimica Acta Part B-Atomic Spectroscopy* **2013**, 87, 139-146.
32. Kellner, P. M.; Dijkstra, H.; Glatzel, U., Quantitative analysis of Mo–Si–B alloy phases with wavelength dispersive spectroscopy (WDS–SEM). *X-Ray Spectrometry*, n/a-n/a.
  33. Li, L. Y.; Li, H.; Qian, M. X.; Strachan, D. M., Gadolinium solubility in peralkaline borosilicate glasses. *Journal of Non-Crystalline Solids* **2001**, 283 (1-3), 237-245.
  34. Li, H.; Li, L.; Vienna, J. D.; Qian, M.; Wang, Z.; Darab, J. G.; Peeler, D. K., Neodymium(III) in aluminoborosilicate glasses. *Journal of Non-Crystalline Solids* **2000**, 278 (1-3), 35-57.
  35. Aleksandrov, L.; Iordanova, R.; Dimitriev, Y., Glass formation in the MoO<sub>3</sub>–Nd<sub>2</sub>O<sub>3</sub>–La<sub>2</sub>O<sub>3</sub>–B<sub>2</sub>O<sub>3</sub> system. *Journal of Non-Crystalline Solids* **2009**, 355 (37–42), 2023-2026.
  36. Aleksandrov, L.; Komatsu, T.; Iordanova, R.; Dimitriev, Y., Study of molybdenum coordination state and crystallization behavior in MoO<sub>3</sub>–La<sub>2</sub>O<sub>3</sub>–B<sub>2</sub>O<sub>3</sub> glasses by Raman spectroscopy. *Journal of Physics and Chemistry of Solids* **2011**, 72 (4), 263-268.
  37. Moncke, D.; Ehrhart, D.; Eckert, H.; Mertens, V., **Influence of melting and annealing conditions on the structure of borosilicate glasses** Influence of melting and annealing conditions on the structure of borosilicate glasses. *Physics and Chemistry of Glasses* **2003**, 44 (2), 113-116.
  38. Sen, S.; Xu, Z.; Stebbins, J. F., Temperature dependent structural changes in borate, borosilicate and boroaluminate liquids: high-resolution <sup>11</sup>B, <sup>29</sup>Si and <sup>27</sup>Al NMR studies. *Journal of Non-Crystalline Solids* **1998**, 226 (1–2), 29-40.
  39. Du, L. S.; Stebbins, J. F., Nature of silicon-boron mixing in sodium borosilicate glasses: A high-resolution B-11 and O-17 NMR study. *Journal of Physical Chemistry B* **2003**, 107 (37), 10063-10076.
  40. Quintas, A.; Charpentier, T.; Majerus, O.; Caurant, D.; Dussossoy, J. L.; Vermaut, P., NMR study of a rare-earth aluminoborosilicate glass with varying CaO-to-Na<sub>2</sub>O ratio. *Applied Magnetic Resonance* **2007**, 32 (4), 613-634.
  41. Stamboulis, A.; Hill, R. G.; Law, R. V., Characterization of the structure of calcium aluminosilicate and calcium fluoro-aluminosilicate glasses by magic angle spinning nuclear magnetic resonance (MAS-NMR). *Journal of Non-Crystalline Solids* **2004**, 333 (1), 101-107.
  42. Neuville, D. R.; Cormier, L.; Massiot, D., Al coordination and speciation in calcium aluminosilicate glasses: Effects of composition determined by <sup>27</sup>Al MQ-MAS NMR and Raman spectroscopy. *Chemical Geology* **2006**, 229 (1–3), 173-185.
  43. Edén, M., Chapter Four - <sup>27</sup>Al NMR Studies of Aluminosilicate Glasses. In *Annual Reports on NMR Spectroscopy*, Graham, A. W., Ed. Academic Press: 2015; Vol. Volume 86, pp 237-331.
  44. McCloy, J.; Washton, N.; Gassman, P.; Marcial, J.; Weaver, J.; Kukkadapu, R., Nepheline crystallization in boron-rich aluminosilicate glasses as investigated by multi-nuclear NMR, Raman, & Mossbauer spectroscopies. *Journal of Non-Crystalline Solids* **2015**, 409, 149-165.
  45. Mullica, D. F.; Lok, C. K. C.; Perkins, H. O.; Benesh, G. A.; Young, V., THE X-RAY PHOTOEMISSION SPECTRA OF ND(OH)(3), SM(OH)(3), EU(OH)(3) AND GD(OH)(3). *J. Electron Spectrosc. Relat. Phenom.* **1995**, 71 (1), 1-20.
  46. Uwamino, Y.; Ishizuka, T.; Yamatera, H., X-RAY PHOTOELECTRON-SPECTROSCOPY OF RARE-EARTH COMPOUNDS. *J. Electron Spectrosc. Relat. Phenom.* **1984**, 34 (1), 67-78.
  47. Farges, F.; Siewert, R.; Brown, G. E.; Guesdon, A.; Morin, G., Structural environments around molybdenum in silicate glasses and melts. I. Influence of composition and oxygen fugacity on the local structure of molybdenum. *Can. Mineral.* **2006**, 44, 731-753.

48. Caurant, D.; Majérus, O.; Fadel, E.; Quintas, A.; Gervais, C.; Charpentier, T.; Neuville, D., Structural investigations of borosilicate glasses containing MoO<sub>3</sub> by MAS NMR and Raman spectroscopies. *Journal of Nuclear Materials* **2010**, 396 (1), 94-101.
49. Du, L.-S.; Stebbins, J. F., Network connectivity in aluminoborosilicate glasses: A high-resolution <sup>11</sup>B, <sup>27</sup>Al and <sup>17</sup>O NMR study. *Journal of Non-Crystalline Solids* **2005**, 351 (43–45), 3508-3520.
50. Wu, J.; Stebbins, J. F., Effects of cation field strength on the structure of aluminoborosilicate glasses: High-resolution <sup>11</sup>B, <sup>27</sup>Al and <sup>23</sup>Na MAS NMR. *Journal of Non-Crystalline Solids* **2009**, 355 (9), 556-562.
51. Inoue, T.; Yokoyama, H., Crystallization on surface layer of high level waste glass. *Denryoku Chuo Kenkyusho Hokoku* **1983**, (282023), 1-28.
52. Zhang, Y. H.; Navrotsky, A.; Li, H.; Li, L. Y.; Davis, L. L.; Strachan, D. M., Energetics of dissolution of Gd<sub>2</sub>O<sub>3</sub> and HfO<sub>2</sub> in sodium alumino-borosilicate glasses. *Journal of Non-Crystalline Solids* **2001**, 296 (1-2), 93-101.
53. Qian, M. X.; Li, L. Y.; Li, H.; Strachan, D. M., Partitioning of gadolinium and its induced phase separation in sodium-aluminoborosilicate glasses. *Journal of Non-Crystalline Solids* **2004**, 333 (1), 1-15.
54. Li, H.; Li, L.; Strachan, D. M.; Qian, M., Optical spectroscopy study of neodymium in sodium alumino-borosilicate glasses. *Journal of Non-Crystalline Solids* **2004**, 349, 127-132.
55. Li, H.; Wang, Z. M.; Li, L. Y.; Strachan, D. M.; Su, Y. L.; Joly, A. G. In *Spectroscopic elucidation of lanthanide cation dissolution mechanism in borosilicate glass*, Symposium on Advanced Fibers, Plastics, Laminates and Composites held at the 2001 MRS Fall Meeting, Boston, Ma, Nov 26-30; Boston, Ma, 2001; pp 291-302.
56. Li, L. Y.; Li, H.; Qian, M. X.; Strachan, D. M., Gadolinium solubility in peraluminous borosilicate glasses. *Journal of Non-Crystalline Solids* **2001**, 281 (1-3), 189-197.
57. Li, H.; Li, L. Y.; Qian, M. X.; Strachan, D. M.; Wang, Z. M., Structure of glass-forming melts - Lanthanide in borosilicates. *Melt Chemistry, Relaxation, and Solidification Kinetics of Glasses* **2005**, 170, 69-80.
58. Li, H.; Li, L. Y.; Strachan, D. M., Structural aspects of Judd-Ofelt oscillator strength parameters: relationship between Nd dissolution and its local environments in borosilicate glasses. *Physics and Chemistry of Glasses* **2005**, 46 (4), 412-419.
59. Li, H.; Su, Y. L.; Li, L. Y.; Strachan, D. M., Raman spectroscopic study of gadolinium(III) in sodium-aluminoborosilicate glasses. *Journal of Non-Crystalline Solids* **2001**, 292 (1-3), 167-176.
60. Quintas, A.; Majerus, O.; Caurant, D.; Dussossoy, J. L.; Vermaut, P., Crystallization of a rare earth-rich aluminoborosilicate glass with varying CaO/Na<sub>2</sub>O ratio. *Journal of the American Ceramic Society* **2007**, 90 (3), 712-719.
61. Nicoleau, E.; Angeli, F.; Schuller, S.; Charpentier, T.; Jollivet, P.; Moskura, M., Rare-earth silicate crystallization in borosilicate glasses: Effect on structural and chemical durability properties. *Journal of Non-Crystalline Solids* **2016**, 438, 37-48.
62. Kidari, A.; Dussossoy, J. L.; Brackx, E.; Caurant, D.; Magnin, M.; Bardez-Giboire, I., Lanthanum and Neodymium Solubility in Simplified SiO<sub>2</sub>-B<sub>2</sub>O<sub>3</sub>-Na<sub>2</sub>O-Al<sub>2</sub>O<sub>3</sub>-CaO High Level Waste Glass. *Journal of the American Ceramic Society* **2012**, 95 (8), 2537-2544.
63. Quintas, A.; Caurant, D.; Majerus, O.; Charpentier, T.; Dussossoy, J. L., Effect of compositional variations on charge compensation of AlO<sub>4</sub> and BO<sub>4</sub> entities and on crystallization



tendency of a rare-earth-rich aluminoborosilicate glass. *Materials Research Bulletin* **2009**, 44 (9), 1895-1898.

64. Qian, M. X.; Li, H.; Li, L. Y.; Strachan, D. M., Extended electron energy loss fine structure simulation of the local boron environment in sodium aluminoborosilicate glasses containing gadolinium. *Journal of Non-Crystalline Solids* **2003**, 328 (1-3), 90-101.

65. Bardez, I.; Caurant, D.; Dussossoy, J. L.; Loiseau, P.; Gervais, C.; Ribot, F.; Neuville, D. R.; Baffier, N.; Fillett, C., Development and characterization of rare earth-rich glassy matrices envisaged for the immobilization of concentrated nuclear waste solutions. *Nuclear Science and Engineering* **2006**, 153 (3), 272-284.

66. Quintas, A.; Caurant, D.; Majerus, O.; Dussossoy, J. L.; Charpentier, T., Effect of changing the rare earth cation type on the structure and crystallisation behaviour of an aluminoborosilicate glass. *Physics and Chemistry of Glasses-European Journal of Glass Science and Technology Part B* **2008**, 49 (4), 192-197.

67. Majerus, O.; Caurant, D.; Quintas, A.; Dussossoy, J. L.; Bardez, I.; Loiseau, P., Effect of boron oxide addition on the Nd<sup>3+</sup> environment in a Nd-rich soda-lime aluminoborosilicate glass. *Journal of Non-Crystalline Solids* **2011**, 357 (14), 2744-2751.

68. Chouard, N.; Caurant, D.; Majerus, O.; Dussossoy, J. L.; Klimin, S.; Pytalev, D.; Baddour-Hadjean, R.; Pereira-Ramos, J. P., Effect of MoO<sub>3</sub>, Nd<sub>2</sub>O<sub>3</sub>, and RuO<sub>2</sub> on the crystallization of soda-lime aluminoborosilicate glasses. *Journal of Materials Science* **2015**, 50 (1), 219-241.

69. Fabian, M.; Svab, E.; Krezhov, K. In Neutron diffraction and RMC modeling of new amorphous molybdate system, *Journal of Physics: Conference Series*, IOP Publishing: 2014; p 012017.

70. Stebbins, J. F.; Ellsworth, S. E., Temperature effects on structure and dynamics in borate and borosilicate liquids: High-resolution and high-temperature NMR results. *Journal of the American Ceramic Society* **1996**, 79 (9), 2247-2256.

71. Sen, S., Temperature induced structural changes and transport mechanisms in borate, borosilicate and boroaluminate liquids: high-resolution and high-temperature NMR results. *Journal of Non-Crystalline Solids* **1999**, 253, 84-94.